Geophysical Research Letters

RESEARCH LETTER
10.1029/2025GL119944

Uncovering the Generation Mechanism of Low-Frequency Chorus Waves (<0.1 f_{ce_eq}) During Active Geomagnetic Environments

Xuan Zhou[1,2], **Xinliang Gao**[1,2], **Dedong Wang**[3], **Jiuqi Ma**[1,2], **and Quanming Lu**[1,2]

[1]CAS Key Lab of Geospace Environment, School of Earth and Space Sciences, University of Science and Technology of China, Hefei, China, [2]CAS Center for Excellence in Comparative Planetology, Hefei, China, [3]GFZ Helmholtz Center for Geosciences, Potsdam, Germany

Key Points:

- We investigate the generation mechanism and global characteristics of low-frequency chorus waves around Earth
- These waves predominantly occur in the MLT range of 0–7 hr and L ~ 6 during storm-time substorms
- Their generation stems from the coexistence of isotropic low-energy and anisotropic high-energy electrons, with a decrease in the magnetic field

Supporting Information:

Supporting Information may be found in the online version of this article.

Correspondence to:

X. Gao,
gaoxl@ustc.edu.cn

Citation:

Zhou, X., Gao, X., Wang, D., Ma, J., & Lu, Q. (2026). Uncovering the generation mechanism of low-frequency chorus waves (<0.1 f_{ce_eq}) during active geomagnetic environments. *Geophysical Research Letters*, *53*, e2025GL119944. https://doi.org/10.1029/2025GL119944

Received 14 OCT 2025
Accepted 9 JAN 2026

Abstract Low-frequency chorus waves (below 0.1 f_{ce_eq}, where f_{ce_eq} is equatorial electron gyrofrequency) can induce the depletion of relativistic electrons in Earth's radiation belts by effective pitch angle scattering, demonstrating distinct effects on radiation belt dynamics compared to typical chorus waves (0.1–0.8 f_{ce_eq}). However, their generation mechanism and environmental drivers remain poorly understood. Analysis of Van Allen Probes data reveals that low-frequency chorus waves predominantly occur in the region of MLT range of 0–7 hr and $L \sim 6$. These waves show a strong correlation with intense substorm activity and moderate magnetic storms, with the majority of waves clustering during storm-time substorms. Their excitation mechanism is driven by the coexistence of isotropic low-energy electrons (below 30 keV) and anisotropic high-energy electrons (above 50 keV) during the storm's peak, along with concurrent geomagnetic field weakening due to enhanced ring currents.

Plain Language Summary Whistler-mode chorus waves are right-hand polarized electromagnetic emissions commonly observed within Earth's magnetosphere, which are well recognized for their dual role in accelerating and scattering radiation belt electrons. Their frequencies typically fall within the range of 0.1–0.8 f_{ce_eq}, making this a widely used identification criterion. However, there also exists another significant population of chorus waves with their frequencies clearly below 0.1f_{ce_eq}. This unique property enables these waves to play a key role in radiation belt electron dynamics, especially by directly precipitating relativistic electrons into the upper atmosphere. Nevertheless, the generation mechanism of low-frequency chorus waves remains debated, with none of the proposed mechanisms adequately accounting for the observations. Using observational data from NASA's Van Allen Probes satellites, we for the first time clearly elucidate the generation mechanism and environmental drivers of low-frequency chorus waves. We find that these waves are excited by the coexistence of isotropic low-energy electrons (<30 keV) and anisotropic high-energy electrons (>50 keV) during concurrent magnetic storms and substorms. This work provides critical insights for advancing predictions of relativistic electron dynamics in the radiation belts.

1. Introduction

Whistler-mode chorus waves are right-hand polarized electromagnetic emissions commonly observed in Earth's magnetosphere (Tsurutani & Smith, 1974). These waves are excited through cyclotron resonance with anisotropic electrons near the magnetic equator (Tsurutani et al., 1979). Typically, chorus waves exhibit two distinct frequency bands, that is, lower (0.1–0.5 f_{ce}, f_{ce} denotes the equatorial electron gyrofrequency) and upper (0.5–0.8 f_{ce}) bands, separated by a 0.5 f_{ce} power gap (Burtis & Helliwell, 1976; Chen et al., 2021; Gao et al., 2019; Santolík, Parrot, et al., 2003; Santolík, Gurnett, et al., 2003). They are known to both precipitate ~keV electrons into the upper atmosphere and accelerate particles to relativistic energies (Agapitov et al., 2019; Gao et al., 2023; Horne et al., 2005; Kasahara et al., 2018; Li et al., 2016; Nishimura et al., 2010; Thorne et al., 2010, 2013). Moreover, the net effect of chorus waves on relativistic electrons depends on their latitudinal distribution (Wang & Shprits, 2019). Intriguingly, chorus waves have also been observed at frequencies below 0.1 f_{ce} in some cases, commonly referred to as low-frequency chorus waves (e.g., Meredith et al., 2014). This distinct population can deplete relativistic electrons through efficient pitch angle scattering, thereby playing a key role in radiation belt dynamics (Gao et al., 2016; Liu et al., 2020).

The spatiotemporal distribution of low-frequency chorus waves was first systematically characterized by Meredith et al. (2014). They proposed that low-frequency chorus waves predominantly arise from propagation effects, wherein chorus waves generated in their source regions propagate into areas with higher magnetic field intensities. Instead, Cattel et al. (2015) suggested that low-frequency chorus waves can be locally excited at frequencies below 0.1 f_{ce_eq} (f_{ce_eq} denotes the equatorial electron cyclotron frequency) in Earth's radiation belts, especially during magnetic storms and prolonged periods of high AE. Up till now, the generation mechanism of the low-frequency chorus waves still remains under debate. Xiao et al. (2017) posited that a high-energy tail population of electrons with relativistic energies can locally excite these waves. Nevertheless, their study was limited to waves with frequencies extending below 0.1 f_{ce_eq}, while their peak frequency still exceeds 0.1 f_{ce_eq}. Recently, He et al. (2022) argued that an increase in plasma density creates favorable conditions for the generation of low-frequency chorus waves. However, this explanation fails to explain why these waves are always prevalent during magnetic storms, as plasma density is usually lower due to the dramatic erosion of the plasmasphere during storms (Thaller et al., 2015). Consequently, none of these theoretical frameworks fully elucidates the underlying processes responsible for the occurrence of low-frequency chorus waves.

In this paper, we comprehensively investigate the generation mechanism and global characteristics of low-frequency chorus waves in Earth's radiation belts using observational data from the Van Allen Probes. First, we conduct a detailed case study to establish the formation process of low-frequency chorus waves and compare their properties with those of typical chorus waves. Next, we perform a statistical analysis to explore the global distribution of these waves and their correlations with geomagnetic activity indices, explaining their prevalence in the radiation belts. The paper is organized as follows: Section 2 describes the data sources and methodology. Section 3 presents the results of the case study and the statistical analysis. Finally, Section 4 summarizes the key conclusions and discusses their implications.

2. Instruments and Data

Van Allen Probes, consisting of two identical satellites, are ideal for studying chorus waves due to their near-equatorial orbits, with a perigee of about 600 km and an apogee of 30,500 km. In our study, the Electric and Magnetic Field Instrument Suite and Integrated Science (EMFISIS) instrument (Kletzing et al., 2013) provides low-resolution (64 samples/s) background magnetic field data. The EMFISIS Waveform Receiver (WFR) offers spectral matrices in the frequency range of 10 Hz–12 kHz. Utilizing the Singular Value Decomposition (SVD) technique (Santolík, Parrot, et al., 2003; Santolík, Gurnett, et al., 2003), we calculate wave planarity and ellipticity to distinguish different plasma waves. The EMFISIS High-Frequency Receiver (HFR) records the upper hybrid resonance frequency, which is used to determine the background cold plasma density. The Energetic Particle, Composition, and Thermal Plasma (ECT) suite (Spence et al., 2013), including the Helium Oxygen Proton Electron (HOPE) and Magnetic Electron Ion Spectrometer (MagEIS), provides the pitch-angle distribution of electrons with energies ranging from dozens of eV to relativistic energies (MeV).

The 1-min resolution solar wind dynamic pressure index, SYM-H index, and AE index are provided by the OMNI database. The geomagnetic model used in this study is a combination of the International Geomagnetic Reference Field (IGRF) and the external field Ts04 model (Tsyganenko & Sitnov, 2005). Using this model, we can obtain the equatorial magnetic field.

3. Results

3.1. Case Study

Figure 1 provides a representative example of the low-frequency chorus waves detected by Van Allen Probe A during a geomagnetic storm that began on 1 November 2012. The red lines in Figures 1e–1h represent the f_{ce_eq}, 0.5 f_{ce_eq}, and 0.1 f_{ce_eq}, respectively. As shown in Figures 1a–1c, the AE index rapidly increased to 600 nT during the development of the storm's main phase (marked by a green rectangle on the top of Figure 1). In this time interval, Van Allen Probe A, operating near the apogee, detected the typical chorus waves where their frequencies follow a value of 0.5 f_{ce_eq} along the satellite's trajectory (Figures 1e–1g). Figure 1h shows the angle (θ_{poyn}) between the wave Poynting flux and the geomagnetic field, as indicative of the wave source region. A θ_{poyn} near zero at MLAT ~3° indicates waves propagating parallel to the magnetic field, confirming that the wave source is near the magnetic equator. As the geomagnetic storm progressed, the AE index continued to rise,

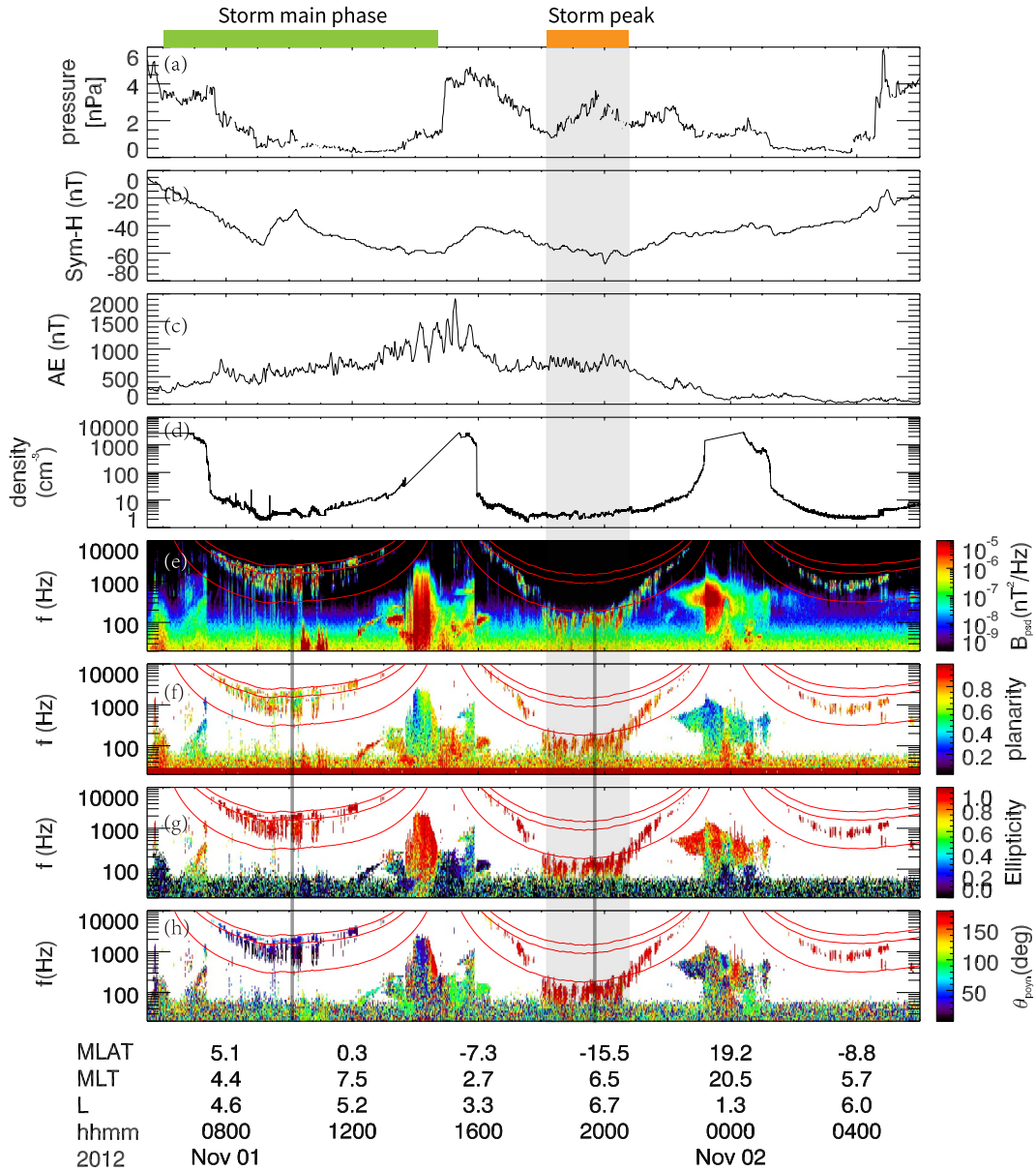

Figure 1. An overview of the low-frequency chorus waves and typical chorus waves from 05:30 UT on 01 November 2012 to 06:00 UT on 02 November 2012 detected by Van Allen Probe A. (a) Solar wind pressure, (b) Sym-H index, (c) AE index, (d) plasma density, (e) magnetic power spectral densities, (f) wave planarity, (g) wave ellipticity, and (h) the angle between the background magnetic field and wave Poynting flux (θ_{poyn}).

reaching 1,500 nT around 15:00 UT. After the outbreak of intense substorms, Van Allen Probe A, operating near L-shell ~6 and MLT ~6, observed a series of chorus waves with frequencies around 100 Hz during the storm's peak (marked by an orange rectangle). The frequency of these waves is surprisingly lower than 0.1 f_{ce_eq}, which are identified as low-frequency chorus waves. The source of low-frequency chorus waves is also near the magnetic equator, as evidenced by a θ_{poyn} value close to 180° in the Southern Hemisphere (MLAT ~ −15°). Additionally, the planarity and ellipticity of low-frequency waves are close to 1, similar to the typical chorus waves.

To investigate the generation mechanism of low-frequency chorus waves, we examine the electron velocity distributions at two times: 10:08:10 UT (t0) when typical chorus waves were observed, and 19:45:00 UT (t1) when low-frequency chorus waves were observed. The electron velocity distributions at t0 and t1 are shown in

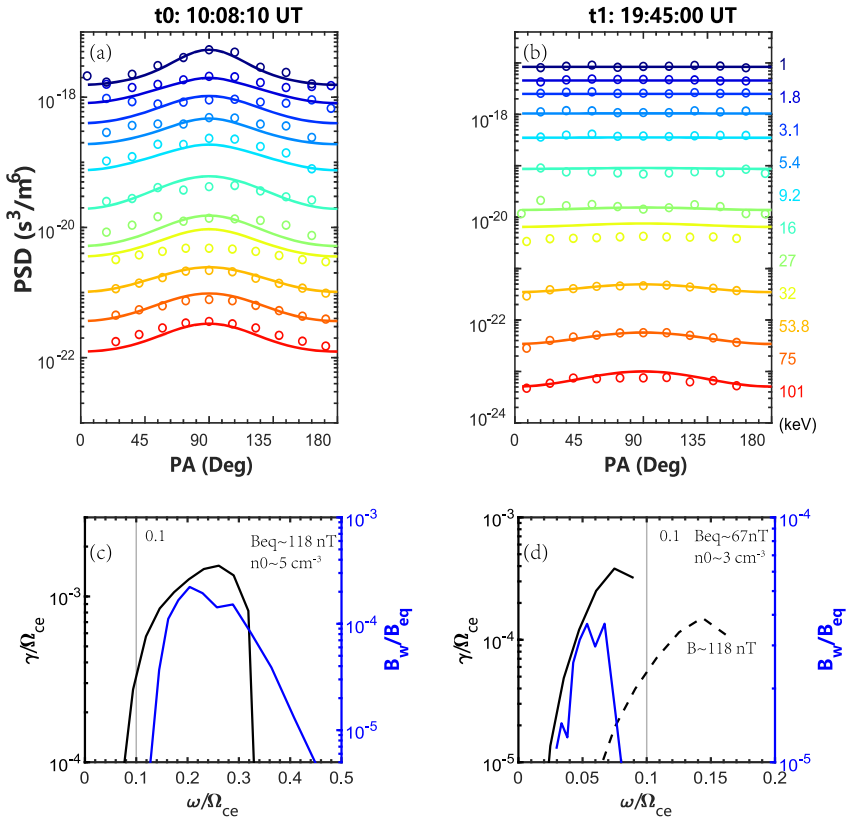

Figure 2. (a, b) Observed (circles) and fitted (lines) electron phase space densities at 10:08:02 (t0) and 19:35:00 (t1) on 01 November 2012 (c, d) The linear growth rates (blue) and the amplitudes (black) of low-frequency chorus waves. The dashed line in panel (d) shows the linear growth rate after increasing the intensity of the geomagnetic field. Ω_{ce} denotes the electron angular gyrofrequency.

Figures 2a and 2b (circles), respectively. At t0, electrons with energies from several keV to hundreds of keV exhibit significant anisotropy. However, at t1, only electrons with energies above 50 keV show anisotropy, while those with lower energies are nearly isotropic. We fit the observations with a multi-component bi-Maxwellian distribution:

$$f_M(v_\parallel, v_\perp) = \sum_j \sqrt{\frac{m}{2T_{\parallel j}\pi}}\ \frac{m}{2T_{\perp j}\pi} n_j e^{-\frac{mv_\parallel^2}{2T_{\parallel j}} - \frac{mv_\perp^2}{2T_{\perp j}}}, \quad (1)$$

where the $m, n_j, T_{\parallel j}$, and $T_{\perp j}$ are the electron mass, electron density, electron parallel temperature, and electron perpendicular temperature for the j th component. The fitted distributions are shown by solid lines in Figures 2a and 2b. Since low-frequency chorus waves are observed at high latitudes (MLAT $\sim -15°$), we further project the local distribution parameters at t1 onto the magnetic equator (source region) by Liouville's theorem. The fitting parameters are listed in Table S1 of Supporting Information S1. Using these parameters, we calculate the linear growth rates with a dispersion relation solver (BO) (Xie, 2019). The linear growth rates (black solid lines) and normalized wave amplitudes (blue lines) for typical chorus waves and low-frequency chorus waves are shown in Figures 2c and 2d, respectively. The amplitudes of typical chorus waves peak at 0.2 f_{ce_eq}, slightly lower than the linear growth rate prediction of 0.26 f_{ce_eq}. This discrepancy likely arises from minor fitting derivations in the 27 and 32 keV electron fluxes measured by the HOPE and MagEIS instruments, respectively. The inconsistency between these two instruments may cause the electron distributions at these energies to deviate slightly from a bi-Maxwellian distribution. However, the amplitudes of low-frequency chorus waves peak at a low frequency of around 0.06 f_{ce_eq}, consistent with the result of linear growth rate (0.07 f_{ce_eq}). The fitting derivations had negligible impact on the low-frequency chorus waves, as both the 27 and 32 keV electrons exhibited nearly

isotropic distributions. All in all, the frequency range of these waves is roughly consistent with that of positive linear growth rates. These characteristics suggest that both waves are locally excited by anisotropic electrons.

These results show that low-frequency chorus waves are excited by anisotropic electrons with energies above 50 keV (Figure 2b), while typical chorus waves are excited by anisotropic electrons with lower energies (minimum resonant energies around several keV). Therefore, we conclude that the frequency disparity between low-frequency and typical chorus waves arises from their distinct free energy sources. The absence of anisotropy in low-energy electrons is crucial for the generation of the low-frequency chorus. If we artificially increase the anisotropy of low-energy electrons at t1, the peak frequency of chorus waves will shift to higher values. Once low-energy electrons become anisotropic, these populations will become the major free energy sources to chorus wave excitation due to their higher density, thereby driving the observed increase in the wave peak frequency. Here, we propose that the formation of isotropic low-energy electrons and anisotropic high-energy electrons may arise from the significant magnetic field depression caused by ring current accumulation during the storm's peak, which will be discussed later.

We also examine the plasma conditions at t0 and t1. At t0, the observed magnetic field (equatorial magnetic field) is 118 nT, and the plasma density provided by the satellite is approximately 5 cm^{-3}. At t1, due to the accumulation of ring current in the storm's peak, the equatorial magnetic field obtained from the Ts04 model decreases to 67 nT, and the plasma density is approximately 3 cm^{-3}, resulting in a larger ratio of f_{pe}/f_{ce_eq} (f_{pe} denotes plasma frequency). A larger ratio of f_{pe}/f_{ce_eq} will lower the peak frequency of wave amplitude (Gary et al., 2012; He et al., 2022). As shown by the dashed line in Figure 2d, if we keep the electron distribution and plasma density constant and increase the magnetic field intensity to 118 nT, the peak frequency of the linear growth rate increases to 0.14 f_{ce_eq} (dashed line in Figure 2d). These results indicate that the weakening of the magnetic field during the storm's peak can directly lead to a decrease in wave frequency by decreasing the value of f_{pe}/f_{ce_eq}. In short, the generation of low-frequency chorus waves results from both the formation of isotropic low-energy electrons and anisotropic high-energy electrons, as well as a decreased magnetic field.

3.2. Statistical Study

In this section, we perform a statistical analysis to explore the global distribution of low-frequency chorus waves and their dependence on background conditions. Firstly, we select the waves that occurred between 1 October 2012 and 31 December 2014, based on observational data from the Van Allen Probes. The following criteria are established: (a) regions with plasma density lower than 124 x $(3/L)^4$ cm^{-3} (Sheeley et al., 2001) and $L > 3$ that are located outside the plasmasphere; (b) waves with planarity >0.5 and ellipticity >0.7 in the frequency range between low hybrid frequency to 0.1 f_{ce_eq} ; (c) at one observational point, the magnetic power spectral densities should be greater than 1e-7 nT^2/Hz in at least five frequency samples, and the wave peak frequency is less than 0.1 f_{ce_eq} ; (d) the angle between the background magnetic field and wave Poynting flux is less than 30° in the northern hemisphere and greater than 150° in the south hemisphere to exclude exohiss wave contamination. Following the same criteria, we also select the lower-band typical chorus waves for comparison, except that their peak frequencies lie between 0.1 and 0.5 f_{ce_eq}. Secondly, we extract the geomagnetic activity conditions during wave occurrence, including the AE index, SYM-H index, and the difference between the observed geomagnetic field and IGRF (*dB*; representing the degree of magnetic field weakening due to ring current enhancement). To investigate the relationship between electron distribution and waves, we finally calculate the electron anisotropy at 5, 10, 20, 32, 54, and 83 keV during wave occurrence. The calculation formula is as follows (Chen et al., 1998):

$$A = \frac{\int_0^{\pi/2} f(\alpha_0) \sin^3\alpha_0 d\alpha_0}{2\int_0^{\pi/2} f(\alpha_0) \cos^2\alpha_0 \sin\alpha_0 d\alpha_0} - 1, \quad (2)$$

where f is the electron's PSD and α_0 is the electron pitch angle for a specific electron energy. For the accurate calculation of the electron anisotropy, we exclude observational points where the electron fluxes detected by the Van Allen Probes have less than nine valid points in pitch angle channels. An anisotropy value (A) of 0 indicates pitch angle isotropy for that specific energy, whereas A greater than 0 indicates pitch angle anisotropy.

The statistical results are displayed in Figure 3, with comparative results for typical chorus waves demonstrated in Figure 4. Figure 3a shows that low-frequency chorus waves primarily occur in the 0–7 MLT sector at $L \sim 6$, in

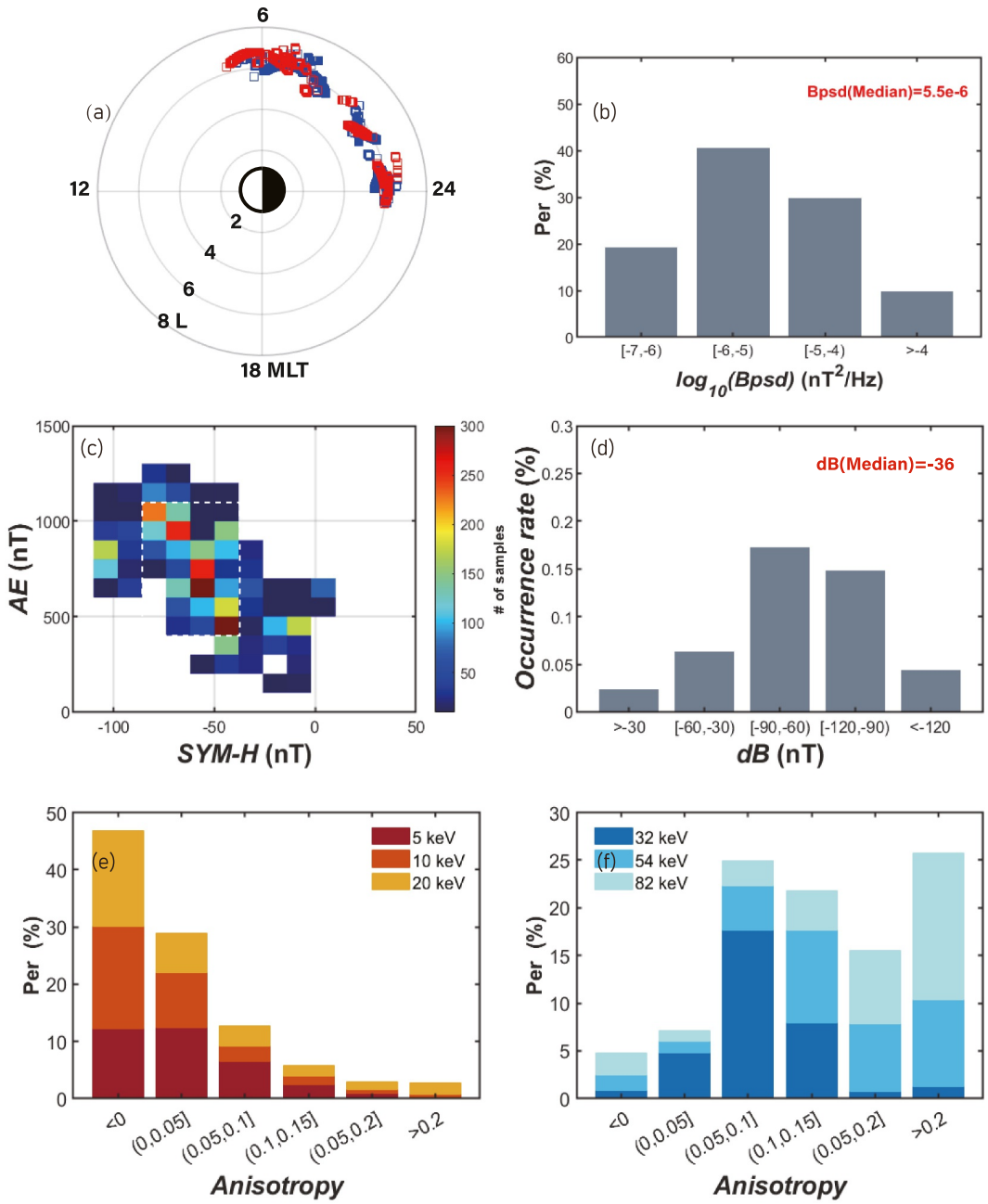

Figure 3. Statistical properties of low-frequency chorus waves and associated background conditions. (a) Distribution of the waves in the MLT-L plane, (b) in SYM-H and AE plane, (f) dependence of the occurrence probability of the difference between the observed geomagnetic field and the IGRF (*dB*), (e) distribution of electrons' anisotropy for 5, 10 and 20 keV, (f) as well as for 32, 54 and 82 keV. The red circles in panel (a) denote data from the Van Allen Probe A, while the blue circles denote data from the Van Allen Probe B.

contrast to typical chorus waves, which are observed across both dayside and nightside regions within the plasmathough (Figure 4a). The magnetic power spectral densities of low-frequency chorus waves (4.4e-6 nT^2/Hz for median value) show comparable intensity with the typical chorus waves (5.5e-6 nT^2/Hz for median value, Figure 4b). Remarkably, the occurrence of low-frequency chorus waves exhibits a pronounced preference for intense substorm activity (median value is 706 nT) and moderate magnetic storms (median value is −58 nT), with the majority of waves clustering during storm-time substorms (Figure 3c, marked by a white rectangle). In contrast, typical chorus waves can still occur during periods of relatively quiet geomagnetic activity, and most of

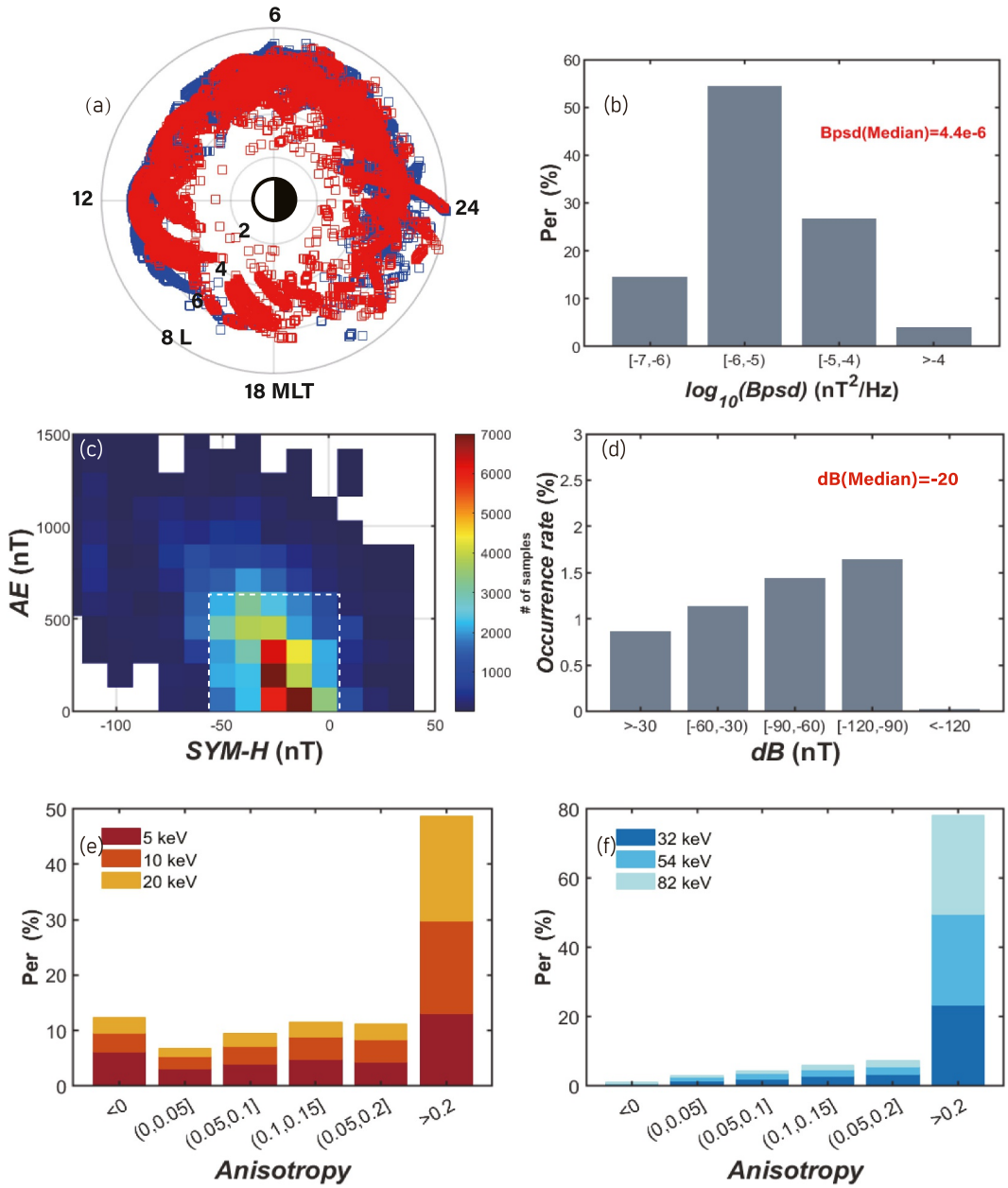

Figure 4. Statistical properties of typical chorus waves and associated background conditions. Figure 4 adopts the same format as Figure 3.

them are concentrated during periods with AE < ~600 nT and SYM-H > ~−60 nT (Figure 4c). The *dB* during low-frequency chorus wave occurrence suggests a significant decrease in magnetic field during the storm time (Figure 3d; median value is −36 nT), which is favorable for the generation of low-frequency chorus waves by leading to a larger f_{pe}/f_{ce_eq}. Differently, the *dB* during typical chorus wave occurrence is higher (Figure 4d). Figures 3e and 3f demonstrate the distribution of electron pitch angle anisotropy across different energy channels during the occurrence of low-frequency chorus waves. As shown in Figure 3e, the anisotropies of electrons at 5, 10, and 20 keV are near or below zero. These electrons lack sufficient anisotropy to provide the free energy required for wave excitation. In contrast, electrons with energies of 32, 58, and 82 keV exhibit significant pitch angle anisotropy, and the electron anisotropy becomes more pronounced as electron energy increases, which can provide sufficient free energies to drive low-frequency chorus waves. Unlike the low-frequency chorus waves, electrons during typical chorus wave occurrence (Figures 4e and 4f) show pronounced anisotropy across all

measured energy ranges (from 5 to 82 keV). These statistical results establish a clear association between the occurrence of low-frequency chorus waves and the coexistence of isotropic low-energy (<30 keV) electrons with anisotropic high-energy (>30 keV) populations. Such a distinctive electron distribution preferentially occurs at L ~ 6 on Earth's dawnside, where the electrons have undergone acceleration from the magnetotail to the inner magnetosphere due to the conservation of the first adiabatic invariant. Furthermore, we proposed that due to the substantial depression of the magnetic field during the storm's peak, electrons with higher energy will gain sufficient energization and exhibit more significant temperature anisotropy.

4. Conclusion and Discussion

This study investigates the generation and global characteristics of low-frequency chorus waves ($<0.1f_{ce\_eq}$) in Earth's radiation belts using Van Allen Probes observations. Low-frequency chorus waves predominantly occur in the MLT range of 0–7 hr and at L ~ 6, exhibiting a localized spatial distribution compared to the broader distribution of typical chorus waves, despite having comparable intensities. These waves exhibit a pronounced preference for intense substorm activity (median value is 706 nT, Figure 3c), and moderate magnetic storms (median value is −58 nT, Figure 3d), with the majority of waves clustering during storm-time substorms. Detailed analysis of electron PSD distributions and plasma conditions reveals that their generation mechanism arises from two concurrent factors: (a) the coexistence of isotropic low-energy electrons and anisotropic high-energy electrons during the storm's peak, and (b) a decrease in geomagnetic field intensity caused by the enhanced ring currents.

The generation of low-frequency chorus waves is robustly related to the intense substorms in the storm's peak. Enhanced ring current buildup during the storm's peak induces pronounced magnetic field depression. This field reduction, similar to the increase in density, will lead to a higher value of f_{pe}/f_{ce_eq}, thereby resulting in a decrease in wave peak frequency (Gary et al., 2012; He et al., 2022). In addition, the intense substorm activities drive intense electron injections into Earth's inner magnetosphere. As these electrons are transported by dawn-dusk electric field from the magnetotail (weaker-field region) to the inner magnetosphere (stronger-field region), they develop anisotropy due to the conservation of the first adiabatic invariant. The resultant energy gain (ΔE) can be expressed as: $\Delta E = \left(\frac{B_{inner}}{B_{tail}} - 1\right) E_{tail}$, where B_{inner} and B_{tail} donate magnetic field intensity in inner magnetosphere and magnetotail, with E_{tail} representing initial electron energy in the magnetotail. During the storm peak, the $\frac{B_{inner}}{B_{tail}}$ reduces due to the enhanced ring current, thereby resulting in electrons with higher initial energies (E_{tail}) to experience a more efficient acceleration process. This acceleration process causes the anisotropy significantly exhibited on high-energy electrons and ultimately drives the generation of low-frequency chorus waves. However, the weaker energy gain of low-energy electrons alone cannot explain their fully isotropic distributions. We speculate that Fermi acceleration plays an equally important role as betatron acceleration due to the rebound of magnetic field lines during transport processes. Nevertheless, the reason why this phenomenon is exclusive to low-energy electrons and is specifically manifested during the main phase of geomagnetic storms warrants further investigation.

Low-frequency chorus waves are absent on the dayside and at lower L-shells, likely due to electron drift motions. When these isotropic low-energy electrons move toward Earth and the dayside by E × B drift as well as curvature and gradient drifts, their anisotropy will increase. The enhanced anisotropy of low-energy electrons will cause an upward shift in wave frequency, explaining the absence of low-frequency chorus waves on the dayside and the smaller L-shell. Our examination of electron PSD across L-shells during period of 19:45 to 22:15 on 1 November 2012 further confirms that lower-energy electrons develop increasing anisotropy with decreasing L (not shown). While the ring current is typically stronger on the dusk side, it is important to note that the free energy required to excite chorus waves and the magnetic field depletion observed in this study both stem from energetic electrons injected at midnight that drift dawnward. As a result, low-frequency chorus waves are concentrated in the dawn sector (MLT ~ 0–7).

Conflict of Interest

The authors declare no conflicts of interest relevant to this study.

Data Availability Statement

The observational data from Van Allen Probes are available from the website https://spdf.gsfc.nasa.gov/pub/data/rbsp/. The OMNI data are obtained from the website http://spdf.gsfc.nasa.gov/pub/data/omni/.

Acknowledgments
This research was funded by the NSFC Grants 42322406 and 42230201, National Key Research and Development Program of China (No. 2022YFA1604600), the "USTC Tang Scholar" program, and the Fundamental Research Funds for the Central Universities (KY2080000063 and KY2080000138). We also acknowledge the entire Van Allen Probes instrument team.

References

Agapitov, O., Mourenas, D., Artemyev, A., Hospodarsky, G., & Bonnell, J. W. (2019). Time scales for electron quasi-linear diffusion by lower-band chorus waves: The effects of fpe/fce dependence on geomagnetic activity. *Geophysical Research Letters*, *46*(12), 6178–6187. https://doi.org/10.1029/2019GL083446

Burtis, W. J., & Helliwell, R. A. (1976). Magnetospheric chorus: Occurrence patterns and normalized frequency. *Planetary and Space Science*, *24*(11), 1007–1024. https://doi.org/10.1016/0032-0633(76)90119-7

Cattell, C. A., Breneman, A. W., Thaller, S. A., Wygant, J. R., Kletzing, C. A., & Kurth, W. S. (2015). Van Allen Probes observations of unusually low-frequency whistler mode waves observed in association with moderate magnetic storms: Statistical study. *Geophysical Research Letters*, *42*(18), 7273–7281. https://doi.org/10.1002/2015GL065565

Chen, H., Gao, X., Lu, Q., Sauer, K., Chen, R., Yao, J., & Wang, S. (2021). Gap formation around 0.5Ωe of whistler-mode waves excited by electron temperature anisotropy. *Journal of Geophysical Research: Space Physics*, *126*(2), e2020JA028631. https://doi.org/10.1029/2020JA028631

Chen, M. W., Roeder, J. L., Fennell, J. F., Lyons, L. R., & Schulz, M. (1998). Simulations of ring current proton pitch angle distributions. *Journal of Geophysical Research*, *103*(A1), 165–178. https://doi.org/10.1029/97JA02633

Gao, X., Chen, L., Li, W., Lu, Q., & Wang, S. (2019). Statistical results of the power gap between lower-band and upper-band chorus waves. *Geophysical Research Letters*, *46*(8), 4098–4105. https://doi.org/10.1029/2019GL082140

Gao, X., Ma, J., Shao, T., Chen, R., Ke, Y., & Lu, Q. (2023). Why chorus waves are the dominant driver for diffuse auroral precipitation. *Science Bulletin*, *69*(5), 2095–9273. https://doi.org/10.1016/j.scib.2023.12.009

Gao, Z., Su, Z., Zhu, H., Xiao, F., Zheng, H., Wang, Y., et al. (2016). Intense low-frequency chorus waves observed by Van Allen Probes: Fine structures and potential effect on radiation belt electrons. *Geophysical Research Letters*, *43*(3), 967–977. https://doi.org/10.1002/2016GL067687

Gary, S. P., Liu, K., Denton, R. E., & Wu, S. (2012). Whistler anisotropy instability with a cold electron component: Linear theory. *Journal of Geophysical Research*, *117*(A7), A07203. https://doi.org/10.1029/2012JA017631

He, Q., Liu, S., Xiao, F., Gao, Z., Li, T., Shang, X., et al. (2022). Observations and parametric study on the role of plasma density on extremely low-frequency chorus wave generation. *Science China Technological Sciences*, *65*(11), 2649–2657. https://doi.org/10.1007/s11431-021-2030-7

Horne, R., Thorne, R., Shprits, Y., Meredith, N. P., Glauert, S. A., Smith, A. J., et al. (2005). Wave acceleration of electrons in the Van Allen radiation belts. *Nature*, *437*(7056), 227–230. https://doi.org/10.1038/nature03939

Kasahara, S., Miyoshi, Y., Yokota, S., Mitani, T., Kasahara, Y., Matsuda, S., et al. (2018). Pulsating aurora from electron scattering by chorus waves. *Nature*, *554*(7692), 337–340. https://doi.org/10.1038/nature25505

Kletzing, C. A., Kurth, W. S., Acuna, M., MacDowall, R. J., Torbert, R. B., Averkamp, T., et al. (2013). The electric and Magnetic Field Instrument Suite and Integrated Science (EMFISIS) on RBSP. *Space Science Reviews*, *179*(1–4), 127–181. https://doi.org/10.1007/s11214-013-9993-6

Li, W., Ma, Q., Thorne, R. M., Bortnik, J., Zhang, X. J., Li, J., et al. (2016). Radiation belt electron acceleration during the 17 March 2015 geomagnetic storm: Observations and simulations. *Journal of Geophysical Research*, *121*(6), 5520–5536. https://doi.org/10.1002/2016JA022400

Liu, S., Xie, Y., Zhang, S., Shang, X., Yang, C., Zhou, Q., et al. (2020). Unusual loss of Van Allen belt relativistic electrons by extremely low-frequency chorus. *Geophysical Research Letters*, *47*(18), e2020GL089994. https://doi.org/10.1029/2020GL089994

Meredith, N. P., Horne, R. B., Li, W., Thorne, R. M., & Sicard-Piet, A. (2014). Global model of low-frequency chorus (fLHR<f<0.1fce) from multiple satellite observations. *Geophysical Research Letters*, *41*(2), 280–286. https://doi.org/10.1002/2013GL059050

Nishimura, Y., Bortnik, J., Li, W., Thorne, R. M., Lyons, L. R., Angelopoulos, V., et al. (2010). Identifying the driver of pulsating aurora. *Science*, *330*(6000), 81–84. https://doi.org/10.1126/science.1193186

Santolík, O., Gurnett, D. A., Pickett, J. S., Parrot, M., & Cornilleau-Wehrlin, N. (2003). Spatio-temporal structure of storm-time chorus. *Journal of Geophysical Research*, *108*(A7), 1278. https://doi.org/10.1029/2002JA009791

Santolík, O., Parrot, M., & Lefeuvre, F. (2003). Singular value decomposition methods for wave propagation analysis. *Radio Science*, *38*, 1010. https://doi.org/10.1029/2000RS002523

Sheeley, B. W., Moldwin, M. B., Rassoul, H. K., & Anderson, R. R. (2001). An empirical plasmasphere and trough density model: CRRES observations. *Journal of Geophysical Research*, *106*(A11), 25631–25641. https://doi.org/10.1029/2000JA000286

Spence, H. E., Reeves, G. D., Baker, D. N., Blake, J. B., Bolton, M., Bourdarie, S., et al. (2013). Science goals and overview of the energetic particle, composition, and thermal plasma (ECT) suite on NASA's Radiation Belt Storm Probes (RBSP) mission. *Space Science Reviews*, *179*(1–4), 311–336. https://doi.org/10.1007/s11214-013-0007-5

Thaller, S. A., Wygant, J. R., Dai, L., Breneman, A. W., Kersten, K., Cattell, C. A., et al. (2015). Van Allen Probes investigation of the large-scale duskward electric field and its role in ring current formation and plasmasphere erosion in the 1 June 2013 storm. *Journal of Geophysical Research: Space Physics*, *120*(6), 4531–4543. https://doi.org/10.1002/2014JA020875

Thorne, R., Li, W., Ni, B., Ma, Q., Bortnik, J., Chen, L., et al. (2013). Rapid local acceleration of relativistic radiation-belt electrons by magnetospheric chorus. *Nature*, *504*(7480), 411–414. https://doi.org/10.1038/nature12889

Thorne, R., Ni, B., Tao, X., & Meredith, N. P. (2010). Scattering by chorus waves as the dominant cause of diffuse auroral precipitation. *Nature*, *467*(7318), 943–946. https://doi.org/10.1038/nature09467

Tsurutani, B. T., & Smith, E. J. (1974). Postmidnight chorus: A substorm phenomenon. *Journal of Geophysical Research*, *79*(1), 118–127. https://doi.org/10.1029/JA079i001p00118

Tsurutani, B. T., Smith, E. J., West, H. I., Jr., & Buck, R. M. (1979). Chorus, energetic electrons and magnetospheric substorms. In P. J. Palmadesso & K. Papadopoulos (Eds.), *Wave instabilities in space plasmas* (Vol. 55–71, pp. 55–62). D. Reidel. https://doi.org/10.1007/978-94-009-9500-06

Tsyganenko, N. A., & Sitnov, M. I. (2005). Modeling the dynamics of the inner magnetosphere during strong geomagnetic storms. *Journal of Geophysical Research*, *110*(A3), A03208. https://doi.org/10.1029/2004JA010798

Wang, D., & Shprits, Y. Y. (2019). On how high-latitude chorus waves tip the balance between acceleration and loss of relativistic electrons. *Geophysical Research Letters*, *46*(14), 7945–7954. https://doi.org/10.1029/2019GL082681

Xiao, F., Liu, S., Tao, X., Su, Z., Zhou, Q., Yang, C., et al. (2017). Generation of extremely low frequency chorus in Van Allen radiation belts. *Journal of Geophysical Research: Space Physics*, *122*(3), 3201–3211. https://doi.org/10.1002/2016JA023561

Xie, H. (2019). BO: A unified tool for plasma waves and instabilities analysis. *Computer Physics Communications*, *244*, 343–371. https://doi.org/10.1016/j.cpc.2019.06.014